④

AD-A199 974

Photoreflectance Study of Boron Ion-Implanted (100) Cadmium Telluride

P.M. AMIRTHARAJ and M. S. ODELL
U.S. Army Center for Night Vision and Electro-Optics
Fort Belvoir, VA 22060

R. C. BOWMAN, JR. and R. L. ALT
Chemistry and Physics Laboratory
The Aerospace Corporation
El Segundo, CA 90245

3 October 1988

Prepared for

SPACE DIVISION
AIR FORCE SYSTEMS COMMAND
Los Angeles Air Force Base
P.O. Box 92960
Los Angeles, CA 90009-2960

DTIC
ELECTE
S
OCT 2 8 1988
D
H

88 1027 037

This report was submitted by The Aerospace Corporation, El Segundo, CA 90245, under Contract No. F04701-85-C-0086-P00019 with the Space Division, P.O. Box 92960, Worldway Postal Center, Los Angeles, CA 90009-2960. It was reviewed and approved for The Aerospace Corporation by S. Feuerstein, Director, Chemistry and Physics Laboratory.

Lt Constance M. Chintall/CNIV was the project officer for the Mission-Oriented Investigation and Experimentation (MOIE) Program.

This report has been reviewed by the Public Affairs Office (PAS) and is releasable to the National Technical Information Service (NTIS). At NTIS, it will be available to the general public, including foreign nationals.

This technical report has been reviewed and is approved for publication. Publication of this report does not constitute Air Force approval of the report's findings or conclusions. It is published only for the exchange and stimulation of ideas.

CONSTANCE M. CHINTALL, Lt, USAF
MOIE Project Officer
SD/CNIV

RAYMOND M. LEONG, Maj, USAF
Deputy Director, AFSTC West Coast Office
AFSTC/WCO OL-AB

AD A199 224

REPORT DOCUMENTATION PAGE

1a. REPORT SECURITY CLASSIFICATION Unclassified			1b. RESTRICTIVE MARKINGS
2a. SECURITY CLASSIFICATION AUTHORITY			3. DISTRIBUTION / AVAILABILITY OF REPORT Approved for public release; distribution unlimited.
2b. DECLASSIFICATION / DOWNGRADING SCHEDULE			
4 PERFORMING ORGANIZATION REPORT NUMBER(S) TR-0088(3945-07)-1			5. MONITORING ORGANIZATION REPORT NUMBER(S) SD-TR-88-89
6a. NAME OF PERFORMING ORGANIZATION The Aerospace Corporation Laboratory Operations		6b. OFFICE SYMBOL (If applicable)	7a. NAME OF MONITORING ORGANIZATION Space Division
6c. ADDRESS (City, State, and ZIP Code) El Segundo, CA 90245-4691			7b ADDRESS (City, State, and ZIP Code) Los Angeles Air Force Base Los Angeles, CA 90009-2960
8a. NAME OF FUNDING / SPONSORING ORGANIZATION		8b. OFFICE SYMBOL (If applicable)	9. PROCUREMENT INSTRUMENT IDENTIFICATION NUMBER F04701-85-C-0086-P00019

8c. ADDRESS (City, State, and ZIP Code)	10. SOURCE OF FUNDING NUMBERS			
	PROGRAM ELEMENT NO.	PROJECT NO.	TASK NO	WORK UNIT ACCESSION NO.

11. TITLE (Include Security Classification)
Photoreflectance Study of Boron Ion-Implanted (100) Cadmium Telluride

12. PERSONAL AUTHOR(S) Amirtharaj, P. M. and Adell, M. S. (Fort Belvoir);
and Bowman, R. C. and Alt, R. L. (The Aerospace Corp.)

13a. TYPE OF REPORT	13b. TIME COVERED FROM_____ TO _____	14. DATE OF REPORT (Year, Month, Day) 3 October 1988	15 PAGE COUNT 23

16 SUPPLEMENTARY NOTATION

17	COSATI CODES		18 SUBJECT TERMS (Continue on reverse if necessary and identify by block number)
FIELD	GROUP	SUB-GROUP	Photoreflectance Modulation Spectroscopy Ion Implantation Effects in Semiconductors Cadmium Telluride II-VI Semiconductor Optical Properties

19. ABSTRACT (Continue on reverse if necessary and identify by block number)

We have studied ion-implanted (100) cadmium telluride using the contactless technique of photoreflectance. The implantations were performed using 50- to 400-keV boron ions to a maximum dosage of 1.5×10^{16} cm^{-2}, and the annealing was accomplished at 500°C under vacuum. The spectral measurements were made at 77 K near the E_0 and E_1 critical points; all the spectra were computer-fitted to Aspnes' theory. The spectral line shapes from the ion-damaged, partially recovered and undamaged, or fully recovered regions could be identified, and the respective volume fraction of each phase was estimated.

20. DISTRIBUTION / AVAILABILITY OF ABSTRACT ☒ UNCLASSIFIED/UNLIMITED ☐ SAME AS RPT. ☐ DTIC USERS	21. ABSTRACT SECURITY CLASSIFICATION Unclassified	
22a NAME OF RESPONSIBLE INDIVIDUAL	22b. TELEPHONE (Include Area Code)	22c. OFFICE SYMBOL

DD FORM 1473, 84 MAR

83 APR edition may be used until exhausted.
All other editions are obsolete.

PREFACE

We wish to thank R. E. Robertson for assistance with the samples and Dr. J. F. Knudsen for the ion implants.

CONTENTS

3

TABLES

FIGURES

I. INTRODUCTION

Ion implantation[1] has been successfully used to fabricate both p- and n-type CdTe[2-5] and to produce controlled amounts of doping in the closely related and important semiconductor alloy $Hg_{1-x}Cd_xTe$.[6,7] Electro-optic devices such as infrared detectors[8] and solar cells[9] have been fabricated using ion-implanted material. However, experimental conditions have not been optimized to obtain the most favorable outcome. The success of implantation doping hinges on optimizing the annealing process subsequent to the implantation: i.e., the post-anneal should remove all the lattice damage caused by energetic ions being projected into the sample and promote defect chemistry that leads to activation of the dopants and suppression of deleterious flaws. Simple and reliable techniques that are capable of providing information on the lattice damage and the electrical behavior are essential to tailoring the annealing process for maximum efficiency.

Photoreflectance (PR),[10-12] the contactless and nondestructive electric-field-modulated reflectivity technique, is well suited for such an application. Differential reflectivity techniques[10-14] are relatively straightforward to implement and are sensitive to lattice damage. In addition, the electric-field-induced changes in the reflectivity contain information regarding the electrical behavior of the semiconductor.[12-14]

We have used PR at 77 K to study (100) CdTe implanted with boron both before and after the annealing process. The heavily damaged zone and regions that are partially or fully recovered due to annealing can be identified using their spectroscopic signatures. In addition we find that, even for a large implant dosage, a small feature characteristic of a relatively undamaged region persists. We have attempted a qualitative order-of-magnitude estimate of the volume fraction of each phase.

The CdTe samples used in this study had already been characterized[15] using a variety of techniques to yield structural and electrical information; these included room temperature photoreflectance, electron paramagnetic

resonance (EPR), neutron depth profiling (NDP), double crystal x-ray diffraction (DCXRD), Rutherford backscattering spectrometry (RBS), and Raman scattering (RS) studies. Careful comparison of the 77-K PR signals observed with other measurements leads to a better understanding of the sample behavior and advances the potential of PR as a characterization tool.

II. EXPERIMENTAL DETAILS

Several bulk (100) CdTe samples were implanted with B^+ ions using different combinations of implantation energies; dosages were chosen to vary the dopant profiles over sufficient depths to reflect a wide range of possible device configurations. The series A samples used four implants with 100, 200, 300, and 400 keV $^{11}B^+$ and a dosage at each energy of 2.5×10^{15} ions cm^{-2}; the series B samples were implanted with two energies, 50 and 100 keV, with a dosage of 5 and 10×10^{15} ions cm^{-2} of $^{10}B^+$, respectively. The post-anneal was performed with samples in evacuated quartz ampoules held at a temperature of ~ 500°C for 1 hour. The implant depths are expected to be ~ 1 and 0.5 μm for the series A and series B sets, respectively. Further details of the implantation procedure may be found in Ref. 15.

The PR measurements were performed at 77 K with a conventional setup[16] that used an He-Ne 6328A laser beam as a pump source; the intensity at the sample surface was ~ 0.5 mW cm^{-2}. The PR line shapes were recorded near the vicinity of the E_0 and the E_1 critical points. The penetration depth of the probe beam in single-crystal CdTe is 0.5 and 0.02 μm, respectively, near the E_0 and E_1 transitions.[17] The sample depth near E_0 is comparable to the implantation range, whereas the E_1 behavior is determined by a shallow near-surface region.

III. RESULTS

The PR spectra measured from the series A ion-implanted samples near E_0 and E_1 are presented in Figs. 1 and 2, respectively. In Fig. 1, the unimplanted/annealed standard sample, labeled S, exhibits a very narrow and intense line shape, as expected from a high-quality single crystal. The implanted/unannealed sample spectrum shown in curve A1 is much broader and weaker in intensity, but with a small sharp feature superimposed on it. On annealing (curve A2), the spectrum increases in intensity, narrows considerably, and develops additional complex structure.

The E_1 spectral line shapes for the same set of samples are shown in Fig. 2. These are considerably simpler and display only one oscillation. The sharpest and most intense is curve S, measured from the unimplanted/annealed standard sample, while the broadest and least intense signal is observed from the implanted/unannealed sample (curve A1). The implanted/annealed sample spectrum falls between curves S and A1 and is shown in curve A2.
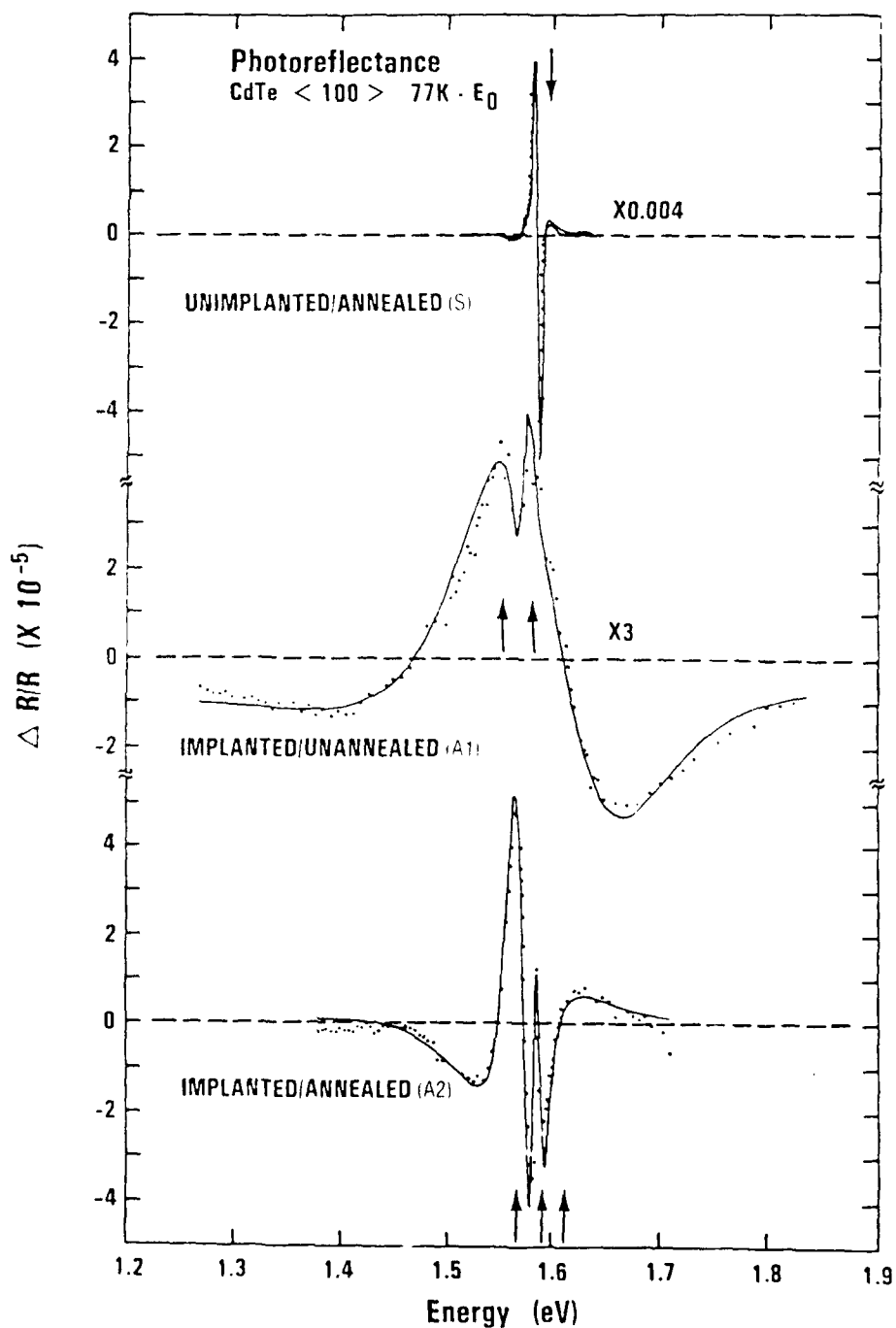
Fig. 1. Photoreflectance Measurements from the Unimplanted and A-Series
Implanted Samples Near the Direct Gap E_0. The solid curve is the
best computer fit to the data; fit values of transition energies are
shown using arrows.
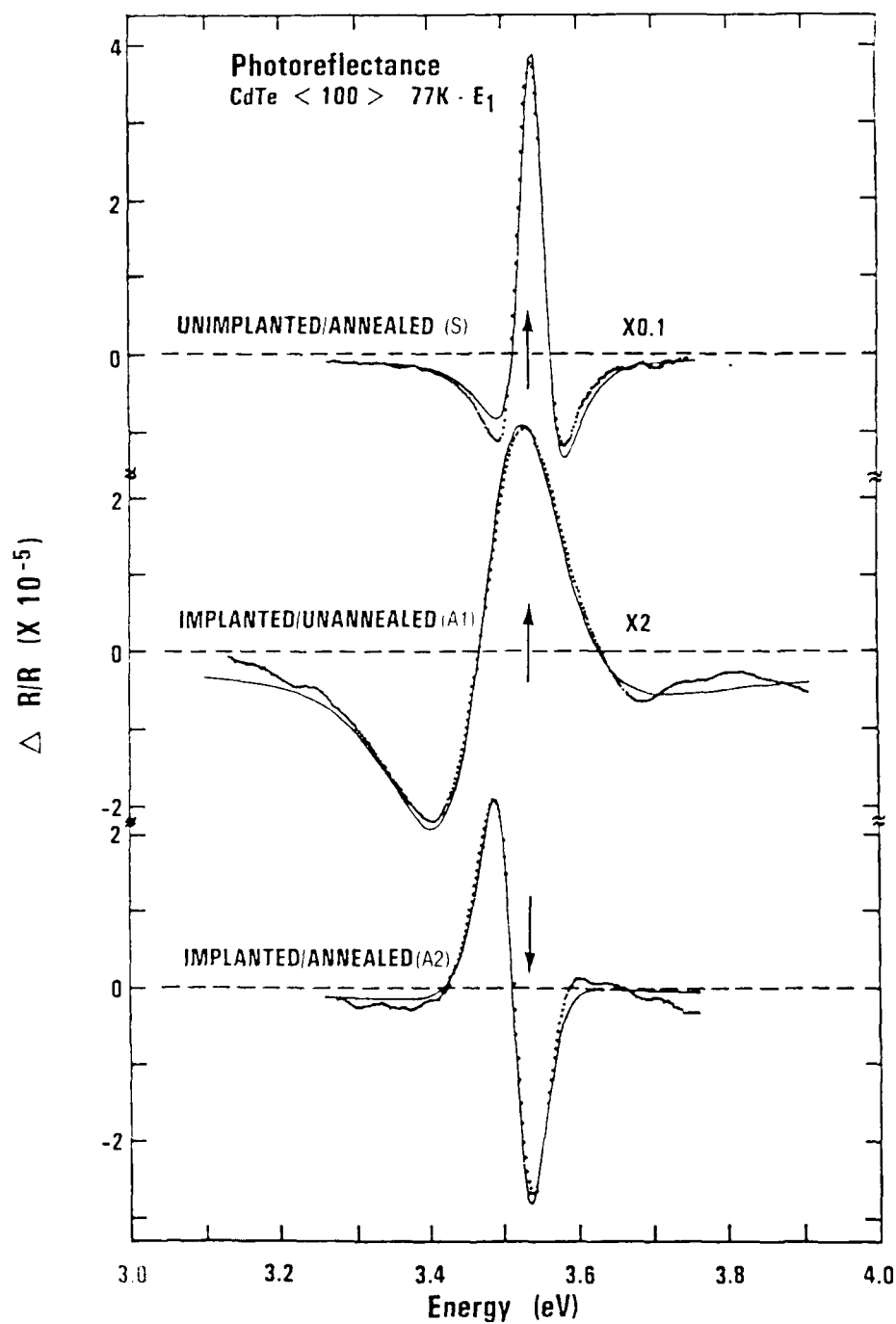
Fig. 2.   Photoreflectance Line Shapes Observed at the E_1 Transition for
A-Series Samples. The reference line shapes measured from the
unimplanted sample is also shown. Results of the computer fit are
shown using a solid line, and transition energies are indicated by
the arrows.

13

IV. DISCUSSION

A. THEORY

The spectra presented in Figs. 1 and 2 were computer-fit applying a
least-squares fitting procedure to the Aspnes' electroreflectance theory;[18]
with multiple contributions, the measured signal $\Delta R/R$ may be expressed as
follows:

$$\Delta R/R(E) = \sum_{j=1}^{m} (1/E^2)C_j L_j + B \tag{1}$$

where

$$L_j = \frac{\cos[\theta_j - (3-n)\Phi_j]}{[(E-E_j)^2 + \Gamma_j^2]^{(3-n)/2}} \tag{2}$$

and

$$\Phi_j = \tan^{-1}\left[\frac{\Gamma_j}{E-E_j}\right] \tag{3}$$

E is the energy and n is a number that depends on the dimensionality of the
critical point. The intensity and phase factors, C_j and θ_j, respectively, are
treated as adjustable parameters along with the transition energy E_j, the
broadening Γ_j, and an energy-independent background B. The intensity factor
C_j depends quadratically on the electric field strength and details of the
band structure near the critical point.

B. E_0 LINE SHAPES

The results of the computer fit for the E_0 line shapes measured from the
series A samples are shown as solid lines in Fig. 1, and the energy gap and
broadening parameter values determined are presented in Table 1. The
unimplanted/annealed sample (curve S) could be well described by a single
sharp and intense line shape, as expected from a good-quality single
crystal. For the implanted/unannealed sample (curve A1), the line shape

Table 1. Parameter Values for the A-Series Implant Samples Determined from a Least-Squares Fit to the Spectra Measured Near the Direct Gap E_0

ID	Description	C_1(eV⁵)	E_{g1}(eV)	Γ_1(meV)	C_2(eV⁵)	E_{g2}(eV)	Γ_2(meV)	C_3(eV⁵)	E_{g3}(eV)	Γ_3(meV)	B
S	Standard-Unimplanted Annealed	7.88×10^{-9}	1.5822	5.9							0.0
A1	Implanted Unannealed				4.72×10^{-11}	1.57	12.0	1.31×10^{-7}	1.590	125.0	-2.34×10^{-6}
A2	Implanted Annealed	9.70×10^{-11}	1.583	9.0	1.94×10^{-9}	1.57	22.0	3.03×10^{-8}	1.56	100.0	0.0
B2	Implanted Annealed (series B)*					1.578	16.0				

*Parameters determined from a three-point fit to the spectrum, using the lowest energy maximum and minimum.

16

becomes much weaker and broadens considerably, as expected from a heavily damaged region.[14] However, a sharp feature is observed superimposed on the broad line shape; this may be due to a crystalline fraction that survived the implantation process or perhaps due to a self-anneal during the implantation. The spectrum was fit using two terms in Eq. (1), representing the crystalline and the heavily damaged regions. On annealing (curve A2), the spectrum becomes more complicated; the spectral line shape suggests a broad and weak oscillation, similar to that observed in sample A1, with two sharp oscillations superimposed on it. A three-term fit may be appropriate in this case, each representing a heavily damaged phase, a partially recovered fraction, and a fully crystallized region.

For the unimplanted standard sample S, the best results were obtained when n was set to zero, the value expected for a two-dimensional (2-D) critical point. The 2-D, instead of the normal 3-D behavior, is expected due to the modification of the nature of the transition by the strong excitonic interaction.[18] The very large intensity also points to a large excitonic contribution. Since all the measurements were performed at 77 K, excitonic contributions will play a much more dominant role than in room-temperature electroreflectance studies. Hence, all the E_0 features were fit using a value of n = 0.

An adjustable constant background term, B, was necessary to obtain a statistically meaningful fit for sample A1. The physical origin of such a background may be the multiple reflection effects that can occur near E_0 due to the changes in the optical constants as a result of heavy damage. The background signal is not an artifact of the measurement procedure.

The spectrum from sample A2 was also measured under optical biasing, using an unchopped laser beam, to investigate the possibility of the observed structure arising from high field Franz-Keldysh (F-K) oscillations.[12,18] The spectrum recorded under bias could be fit with the same transition energies and broadening parameters, but reduced intensity factors. No change in the oscillation period expected from F-K oscillations was observed. This suggests that the sample behavior is consistent with the description used here.

17

The overall quality of all the fits was good. The energy gap and broadening parameter values determined from the fit for the unimplanted sample are in good agreement with earlier observations.[19] In light of the previous results[15] on these boron-implanted CeTe samples, the presence of the undamaged phase in sample A1 is unexpected. Getting et al. have reported that implantations to dosages of 5×10^{16} ions cm^{-2} with various heavy ions failed to produce amorphous CdTe. Raman scattering and RBS measurements on similar boron-implanted samples also suggest the presence of a residual crystalline region near the surface.[15] Of course, the sharp PR signal could have also originated in the undamaged region beyond the boron implant range.

The behavior of the B series samples was different from that of the A series, perhaps as a result of the heavier implant dose. The spectra from the implanted unannealed B series sample, B1, were too broad and weak to warrant a careful study. The line shape from sample B2 that had been implanted and annealed was similar to those observed under high field conditions with a large F-K contribution.[12,18] No detailed fit was justifiable in this case. Hence, the lowest minimum and maximum, along with a three-point fit method,[18] were used to estimate the dominant transition energy and its associated broadening parameter. These values are also shown in Table 1 and are comparable with those of the partially recovered phase in sample A2.

C. E_1 LINE SHAPES

The behavior of the spectral line shapes in the vicinity of the E_1 critical point are simpler and more straightforward than those discussed in the previous section. As seen in Fig. 2, only a single set of oscillations and, hence, a single transition was observed. All the spectra could be fit using one 2-D critical point. A constant background was used in all the samples. The fit results are shown as solid curves in Fig. 2, and the transition energy (E_j), broadening parameter (Γ_j), background (B), and intensity factors (C_j) determined from the fits are presented in Table 2.

Table 2. Parameter Values Determined from a Least-Squares Fit to
the Spectra Measured Near the E_1 Critical Point

ID	Description	C (eV^5)	E_g(eV)	Γ(meV)	B
S	Standard - Unimplanted Annealed	1.38×10^{-7}	3.543	46.0	-8.24×10^{-6}
A1	Implanted Unannealed	5.94×10^{-7}	3.494	145.0	-1.37×10^{-6}
A2	Implanted Annealed	8.70×10^{-8}	3.51	56.8	-1.0×10^{-6}
B2	Implanted Annealed (series B)	7.63×10^{-8}	3.478	92.5	1.75×10^{-6}

The unimplanted/annealed crystalline sample, S, displays a sharp E_1
spectral feature. The implanted sample A1 exhibits a very broad and weak line
shape. The fit parameter for the implanted and annealed samples are much
closer to S than to A1, suggesting a substantial degree of recovery. The fit
to the spectrum from sample B2 of the heavier implant series was poor, most
likely due to the presence of the large electric field apparent in the E_0 line
shape behavior. The spectrum from the implanted/unannealed sample B1, as in
the case of E_0, was too broad and weak and hence not studied. The constant
background was comparable to the noise in the spectra for all samples except
for A1.

D.   SHIFTS IN E_0 AND E_1 WITH IMPLANTATION AND ANNEALING

The three E_0 energy values observed in the A series and the sample-to-sample variation in the E_1 energy may be significant and reveal additional information regarding the state of the implanted and annealed regions. Lattice damage, local strains, electric fields, and large concentration of dopants may lead to changes in the measured optical transition energies. The sharpest component in sample A3, in the vicinity of E_0, occurs at the same energy as that in the unimplanted sample and clearly originates in a region that has undergone a substantial degree of recovery; the broader line width may indicate that the recovery is not complete. The 1.57-eV feature, with a larger broadening parameter of 12 to 22 meV, may originate in a partially recovered fraction or recovered regions subjected to local strains and electric fields. The broadest E_0 component in samples A1 and A2 must originate in the heavily damaged zone. The large line widths, and additional features in the case of sample A2, reduce the accuracy with which the transition energy value of the broadest component can be established. However, the upshift in sample A1 is probably reliable and may be the result of a net compressional stress exerted by the large density of implant species.[20]

The reduction of the E_1 energy with the corresponding broadening parameter suggests that, the larger the deviation from crystallinity, the lower the E_1 energy. Ion damaged Si[21] and GaAs[14] exhibit a decrease and increase, respectively, in the E_1 energy with implantation dosage. However, these are suspected to be a result of the large doping densities and not directly related to the ion damage. In the samples studied, it has been shown that the implantation and annealing leads to minimal activation[15] of the dopants, and the E_1 down shifts are probably directly related to the implantation damage. The details of the mechanisms that cause the shift, however, are not well understood.

E.   CRYSTALLINE VOLUME FRACTION

The volume fraction of the crystalline phase in a sample subjected to implantation and annealing is an important parameter. The three intensity factors that determine the individual contribution of the three possible phases, i.e., undamaged or fully recovered, partially recovered, and heavily damaged, may contain some information regarding the volume fractions of these individual phases. Even though the measurement conditions were identical in all the cases, sample-to-sample comparisons of the values of C_j shown in Tables 1 and 2 are not valid due to the differences that could be present in their electronic properties; qualitative comparison of two phases within the same sample may be more reasonable. In the simplest approximation, if one assumes that there are only three phases and that they are distributed uniformly throughout the sampling volume, then the values of C_j should be directly proportional to the volumes of their respective phases. However, an examination of the E_1 line shapes shows that the recovery for sample A2 is almost complete, leading to the conclusion that the near-surface region is nearly crystalline. This suggests that the degree of recovery may be larger near the surface. The lower damage probability from the projected range calculations[22] and $^{10}B^+$ profiling using NDP measurements[15] are consistent with this conclusion. The volume fraction of the crystalline phase determined from considering only the value of C_j in sample A2 would therefore be an overestimate. These arguments, along with a value of C_1/C_3 of ~ 10^{-3} in sample A2, and values of C_2/C_3 of ~ 10^{-1} in samples A1 and A2, respectively, strongly suggest that the volume fraction of the undamaged or recovered phases are small. It is clear that the strength of PR and other forms of electric-field-modulated reflectivity techniques lies in the fact that such small fractions of the crystalline phase can be detected. The disadvantage, on the other hand, is that the damaged regions are much more difficult to observe.

V. CONCLUSIONS

We have investigated ion damage in boron-implanted CdTe both before and after annealing, using photoreflectance; an unimplanted sample was studied under identical conditions to provide a comparison standard. Detailed line shape analyses at the E_0 optical transition reveal the presence of three phases: namely, the ion damaged, partially recovered and undamaged, or fully recovered. All three phases were present in the implanted and annealed sample, whereas only two were observed in the implanted sample. The behavior of the E_1 line shape suggests that the recovery near the surface due to annealing is significantly larger. An estimate of the recovered crystalline fraction suggests that, in the implanted and annealed sample, the volume fraction of the fully and partially recovered phases are $< 10^{-3}$ and $< 10^{-1}$, respectively. The strength of PR is in its ability to detect such small crystalline fractions. The results presented here are consistent with earlier studies of the same samples, using a variety of structural and electrical probes.

REFERENCES

1. T. W. Sigmon, Nucl. Instru. Methods B 7/8, 402 (1985).

2. M. Gettings and K. G. Stephens, Radiat. Eff. 22, 53 (1974).

3. M. Chu, R. H. Bube, and J. F. Gibbons, J. Electrochem. Soc. 127, 483 (1980).

4. C. B. Yang, J. T. Lue, H. L. Hwang, and M. L. Peng, IEEE Tran. Electron Devices ED-32, 2297 (1985).

5. R. Kalish, M. Deicher, and G. Schatz, J. Appl. Phys. 53, 4793 (1982).

6. G. L. Destefanis, Nucl. Instrum. Methods 209/210, 567 (1983).

7. L. O. Bubulac, D. S. Lo, W. E. Tennant, D. D. Edwall, and J. C. Robinson, J. Vac. Sci. Technol. A 4, 2169 (1986).

8. M. B. Reine, A. K. Sood, and T. J. Tredwell, Semiconductors and Semimetals, Vol. 18, eds., R. K. Willardson and A. C. Beer (Academic, New York, 1981), p. 201.

9. M. Chu, A. L. Fahrenbruch, R. H. Bube, and J. F. Gibbons, J. Appl. Phys. 49, 322 (1978).

10. R. C. Bowman, Jr., R. L. Alt, and K. W. Brown, "Modern Optical Characterization Techniques for Semiconductors and Semiconductor Devices," eds., O. J. Glembocki, F. H. Pollak, and J. J. Song, Proc. SPIE, 794, 94 (1987).

11. G S. Eidzhyunas, Yu. F. Kavalyauskas, and A. Yu. Shileika, Sov. Phys. Semicond. 20, 499 (1986).

12. W. M. Duncan and A. F. Schreiner, Solid. State Commun. 31, 457 (1979).

13. D. D. Sell and A. U. MacRae, J. Appl. Phys. 41, 4929 (1970).

14. R. L. Brown, L. Schoonfeld, L. L. Abels, S. Sundaram, and P. M. Raccah, J. Appl. Phys. 52, 2950 (1981).

15. R. C. Bowman, Jr., R. L. Alt, P. M. Adams, J. F. Knudsen, D. N. Jamiesen, and R. G. Downing, J. Cryst. Growth 86, 768 (1988).

16. P. M. Amirtharaj, J. H. Dinan, J. J. Kennedy, P. R. Boyd, and O. J. Glembocki, J. Vac. Sci. Technol. A 4, 2028 (1986).

17. L. Vina, C. Umbach, M. Cardona, L. Vodopyanov, <u>Phys. Rev. B</u> <u>29</u>, 6752 (1984).

18. D. E. Aspnes, <u>Handbook on Semiconductors</u>, Vol. II, ed., M. Balkanski (North-Holland, New York, 1980), p. 109.

19. J. J. Kennedy, P. M. Amirtharaj, P. R. Boyd, S. B. Gadri, R. C. Dobbyn, and G. G. Long, <u>J. Cryst. Growth</u> <u>86</u>, 93 (1988).

20. V. I. Gavrilenko, V. A. Zuev, and V. G. Litovchenko, <u>Sov. Phys. Solid State</u> <u>19</u>, 333 (1977).

21. D. E. Aspnes, G. K. Celler, J. M. Poate, G. A. Rozgonyi, and T. T. Sheng, <u>Symposium on Laser and Electron Beam Processing of Electronic Materials</u>, Electrochemical Society Proc., Vol. 80-1, p. 414 (1980).

22. J. F. Gibbons, <u>Handbook on Semiconductors</u>, Vol. III, ed., S. P. Keller (North-Holland, New York, 1980), p. 599.

LABORATORY OPERATIONS

The Aerospace Corporation functions as an "architect-engineer" for national security projects, specializing in advanced military space systems. Providing research support, the corporation's Laboratory Operations conducts experimental and theoretical investigations that focus on the application of scientific and technical advances to such systems. Vital to the success of these investigations is the technical staff's wide-ranging expertise and its ability to stay current with new developments. This expertise is enhanced by a research program aimed at dealing with the many problems associated with rapidly evolving space systems. Contributing their capabilities to the research effort are these individual laboratories:

Aerophysics Laboratory: Launch vehicle and reentry fluid mechanics, heat transfer and flight dynamics; chemical and electric propulsion, propellant chemistry, chemical dynamics, environmental chemistry, trace detection; spacecraft structural mechanics, contamination, thermal and structural control; high temperature thermomechanics, gas kinetics and radiation; cw and pulsed chemical and excimer laser development including chemical kinetics, spectroscopy, optical resonators, beam control, atmospheric propagation, laser effects and countermeasures.

Chemistry and Physics Laboratory: Atmospheric chemical reactions, atmospheric optics, light scattering, state-specific chemical reactions and radiative signatures of missile plumes, sensor out-of-field-of-view rejection, applied laser spectroscopy, laser chemistry, laser optoelectronics, solar cell physics, battery electrochemistry, space vacuum and radiation effects on materials, lubrication and surface phenomena, thermionic emission, photosensitive materials and detectors, atomic frequency standards, and environmental chemistry.

Computer Science Laboratory: Program verification, program translation, performance-sensitive system design, distributed architectures for spaceborne computers, fault-tolerant computer systems, artificial intelligence, microelectronics applications, communication protocols, and computer security.

Electronics Research Laboratory: Microelectronics, solid-state device physics, compound semiconductors, radiation hardening; electro-optics, quantum electronics, solid-state lasers, optical propagation and communications; microwave semiconductor devices, microwave/millimeter wave measurements, diagnostics and radiometry, microwave/millimeter wave thermionic devices; atomic time and frequency standards; antennas, rf systems, electromagnetic propagation phenomena, space communication systems.

Materials Sciences Laboratory: Development of new materials: metals, alloys, ceramics, polymers and their composites, and new forms of carbon; nondestructive evaluation, component failure analysis and reliability; fracture mechanics and stress corrosion; analysis and evaluation of materials at cryogenic and elevated temperatures as well as in space and enemy-induced environments.

Space Sciences Laboratory: Magnetospheric, auroral and cosmic ray physics, wave-particle interactions, magnetospheric plasma waves; atmospheric and ionospheric physics, density and composition of the upper atmosphere, remote sensing using atmospheric radiation; solar physics, infrared astronomy, infrared signature analysis; effects of solar activity, magnetic storms and nuclear explosions on the earth's atmosphere, ionosphere and magnetosphere; effects of electromagnetic and particulate radiations on space systems; space instrumentation.